Niklas Petry, Dominik Schäfer, Oliver Lammel, Fabian Hampp, Quantification of coflow effects on primary atomization of pressure swirl atomizers, International Journal of Multiphase Flow 149 (2022) 103946

The original publication is available at www.elsevier.com

https://doi.org/10.1016/j.ijmultiphaseflow.2021.103946

Quantification of co-flow effects on primary atomization of pressure swirl atomizers

Niklas Petry, Dominik Schäfer, Oliver Lammel, Fabian Hampp*

German Aerospace Center (DLR),
Institute of Combustion Technology,
Pfaffenwaldring 38-40, D-70569 Stuttgart, Germany

Abstract

This work investigates the bilateral interactions between a coaxial air flow and the primary atomization process of a liquid spray generated by pressure-swirl atomizers. For the experimental investigation a generic test section with large optical access is used. The ambient conditions were kept consistent to afford a certain amount of comparability in each investigated case. High momentum jet stabilized combustors based on the FLOX® burner concept are used successfully in gas turbines due to its fuel and load flexibility and very low pollutant emissions. In previous and ongoing studies, different model combustors have been under investigation mainly with the focus of broadening fuel flexibility and operational limits. Operation with different liquid fuel injection systems in high pressure experiments showed a significant impact from the injector shape and injection strategy on the fuel air mixing behavior, the flame position and stability, and thus NOx emissions. This experiment will give a more detailed understanding of the turbulent mixing and interaction of primary atomization with the surrounding air in such burners. The setup will also allow for the testing of different injection systems for various burner configurations by the variation of injection type, location, fuel, and air flow properties. In the present experiments a pressure-swirl atomizer operates at a constant pressure drop and mass flow. Liquid fuel was replaced by deionized water due to safety concerns. The coaxial

*Corresponding author
Email address: fabian.hampp@dlr.de (Fabian Hampp)

air mass flow was set to bulk velocities of 20 m/s, 35 m/s, 50 m/s, and 80 m/s. A modified Particle Image Velocimetry (PIV) with phosphor-particles was used to characterize the flow field near by the liquide-gas interface and also downstream of the point of injection. The sinuous wave character of the instabilities and the growth rate of the initially small perturbations is visualized by shadowgraphy techniques. Here, the significant behaviour is quantified by parameters, which allows comparing different injector types. The results show significant influence of the aerodynamic forces on the growth rate with increasing co-flow velocities. The spray cone angle widens at high co-flow velocities due to static pressure drop in the flow field. Therefore the break-up length shortened at high velocities due to the larger tangential shear rate. This leads to larger droplets, as a result of mass conservation approach. It is also shown that the surrounding flow field gets deflected by the liquid sheet and initalized turbulences downstream.

These findings assist the ongoing developments of liquid fuel injection systems for high momentum jet based combustors and provide validation data for numerical simulations of primary and secondary atomization.

Keywords: high momentum jet flames, FLOX®, gas turbine combustion, pressure swirl atomizer, atomization, primary breakup, multiphase measurement, particle image velocimetry, shadow imaging

---

INTRODUCTION

In reference to the political target in peripheral energy supply, development of micro gas turbines becomes more relevant. Especially to conform the requirements in pollutant emissions, the injection process in high momentum jet stabilized combustors has been investigated in detailed studies.[**?**].... The premixed fuel-air injection is generated by a pressure-swirl atomizer. A swirled conical sheet is located downstream the nozzle exit and interferes with the coaxial air flow, due to viscous shear forces among the two phases, distortions on the liquid sheet become excited. At this point the kelvin-helmholtz instabilities lead to breakup and therefore small droplets. For a better understanding of primary breakup mechanism the bilateral interaction between jet and fluid is of particular importance.

Basically the process of atomization is apportionable in four regimes. The regime close to the nozzle exit is called the primary breakup and is part of the following investigations. The second regime is called dense regime and includes the formation of ligaments and droplets. In the intermediate and dilute regime breakup into small droplets takes place and a homogeneous mixture is existent. According to this a high surface area is availiable and results in an enhanced ignition behavior with less pollutant emissions.

The application of pressure swirl atomizers occurs in gas turbines, industrial combusters, rocket engines, diesel engines and many other technical fields. The principle of converting pressure into kinetic energy is highly efficent and results in a homogeneous mixture. The breakup takes place due to the lack in velocity among liquid and gas flow. The typical conical sheet is formed by the centrifugal forces of the swirl afflicted liqiud. Even the swirling flow flied is attached at the wall of the inner chamber and leaves the orifice as a thin liquid film.

Previous studies investigated the mechanism of primary breakup, thereby mathematical modells were developed and numerical simulations indicated the turbulent influences on the breakup process. cite/shäfer shows in his paper the distribution and dispersion of droplets in the turbulent flow field with different

co-flow velocities. To obtain a verification set of data for numerical simulations, the field was observed with laser based measurement techniques in a generic test section. In consideration of two phase flows, particle imaging velocimetry techniques are non-trivial and not widely-used. The studies of [**?**] are concerned with determining the velocimetry of droplets on the basis of mie-scattering signals. A simultaneous measurement of a coaxial flow flied and liquid phase is the aim of the present work.

In the work presented here, a modified particle imaging velocimetry technique is used to visualize and quantify the flow field for different co-flow velocities. Thereby the selection of tracer particles to satisfy the operational requirements is a matter of particular interest.

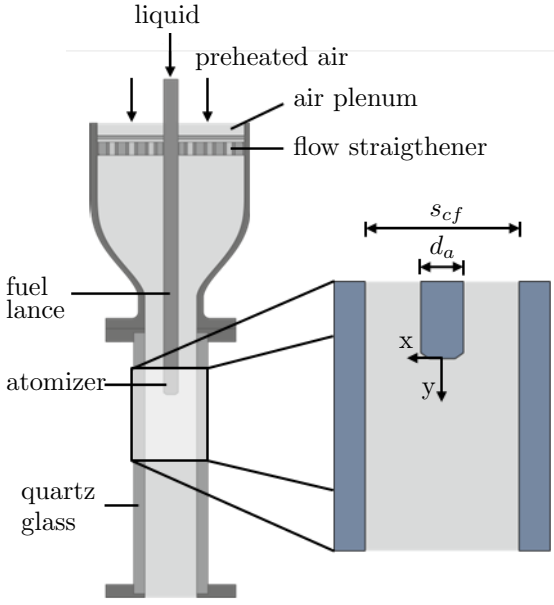

Figure 1: **Measurement section and flow channel dimensions**

EXPERIMENTAL SETUP

The measurement section and the flow channel are schematically depicted in Fig. 1 and goes back to the investigations of [**?**]. The test section is divided into

two parts. First, the contraction nozzle with flow straightening elements and second, the measurement section with optical access. The measurement section has a rectangular cross-section of $A_{cf} = 40\,\text{mm} \times 40\,\text{mm}$ and a total length of 200 mm. Quartz glass windows confine the measurement section from all four sides. The size of the outline is a trade-off between available air quantity and distance between injector and window. Surface wetting is attempted to avoid or shifted downstream to aid optical access to the spray region. Therefore modifactions were made in the flow channel. A wall filmmaker was mounted between the contraction nozzle and measurement section. Due to this additional flow a thin boundary is formed on the window and enables an enhanced optical access in the spray region. Especially for PIV investigations a certain time range is necessary to provide highly resolved measurements.

The flow channel is supplied by different peripheral devices that are not shown in Fig. 1. Air is supplied by a compressor and the flow rate is regulated by a mass flow controller (Bronkhorst EL-Flow series). An air preheating system with 38 kW electrical power is used for preheating the additional air flow in the wll filmmaker (maximum temperature 723 K). The liquid is supplied by a stainless steel cylinder pressurized by nitrogen. The gas and liquid phase in the supply cylinder are separated by a piston. The liquid mass flow is controlled via a mass flow controller (Bronkhorst mini CORI-FLOW M14) and guided into the fuel lance system. Behind the test section, the multiphase flow is cooled and liquid fuel droplets are separated by means of a wire mesh demister.

Different injection systems can be mounted onto the fuel lance in the centre of the duct (i.e. for full-scale injector testing) or into an alternative metal window plate (e.g. for single jet-in-crossflow type tests). A cooling jacket inside the fuel lance system maintains the injection temperature and thus surface tension and viscosity constant at varying airflow conditions. This is necessary to provide consistent atomization from the injector at different operational points. Fuel temperature is measured by a k-type thermocouple at the tip of the fuel lance directly at the inflow of the atomizer.

In the current study, two hollow cone pressure swirl atomizers (type: Schlick

V121 and Delavan D27710-3) with a nominal spray angle of 60° were mounted coaxially onto the tip of the fuel lance, facing downstream in the direction of the air flow. The atomizers have a discharge orifice diameter of $d_{Schlick,0} = 0.15\,\text{mm}$, $d_{Delavan,0} = 0.35\,\text{mm}$ and an outer diameter of $d_a = 12\,\text{mm}$. The outer diameter corresponds to the fuel lance diameter in order to keep the upstream air flow unaffected. The injectors have a flat tip and the discharge orifice is located in the centre.

Operating Conditions

The operational parameters of the ambient air flow are shown in Tab. 1. The bulk air flow velocity is adjusted to 20 m/s, 35 m/s, and 50 m/s for three different operating points OP2, OP3 and OP5, respectively. The preheated air temperature is set to a constant value of $T_a = 298\,\text{K}$ for all OPs. This corresponds to Reynolds numbers (Re_a) range from $5.3{\times}10^4$ to $1.3{\times}10^5$ of the turbulent ambient air flow.

Deionized water is used as a replacement for liquid fuel due to safety concerns. The water mass flow is set to a constant value of $\dot{m}_a = 0.4\,\text{g/s}$ which corresponds to a pressure differential across the atomizer of $\Delta P_{l,Schlick} = 11\,\text{bar}$ and $\Delta P_{l,Delavan} = 6.5\,\text{bar}$. Fuel lance cooling is regulated to a liquid injection temperature at the atomizer inflow of $T_l = 298\,\text{K}$.

	$\dot{m}_a$ [g/s]	T_a [K]	Re_a	$\overline{u}_a$ [m/s]
OP20	23.5	298	$5.3{\times}10^4$	20
OP50	59.0	298	$9.3{\times}10^4$	35
OP80	94.5	298	$1.3{\times}10^5$	50

Table 1: **Operational parameters of ambient air**

MEASUREMENT TECHNIQUES

Particle Image Velocimetry

Particle Image Velocimetry (PIV) is applied to visualize the multiphase flow field downstream from the point of injection. Two flash lamp pumped frequency-doubled Nd:YAG lasers with a LBO-crystal, to excite the third harmonic($\lambda = 355\,\mathrm{nm}$), are used for the particle illumination. The laser beams are converted into a 30 mm high laser light sheet and guided vertically into the flow channel. The light sheet thickness inside the flow channel is approximately 200 µm. The lasers are triggered at 10 Hz with a beam separation time of $\Delta t = 10\,\mu s$ for OP2 and OP3/5, respectively.

The scattered light from the particles is imaged with a double frame CCD camera (LaVision Imager SX 9M) with 3360 × 2712 pixels. The camera is triggered synchronously to the lasers at 10 Hz and timed by a programmable timing unit (LaVision PTU-X). The camera is equipped with a Tokina macro lens with a focal length of 100 mm and a broad band filter with a transmission range at around $355 \pm 5\,\mathrm{nm}$. The resulting field of view (FOV) is 30 mm × 20 mm and the pixel resolution is calculated with 9 µm per pixel.

Barium magnesium aluminate, europium doped particles with a nominal diameter of 2-5 µm are used for seeding the airflow. The seeded airflow is guided into the main airflow directly after the preheat system, approximately 1.5 m upstream of the measurement locations. Depending on the OP, carrier mass flow through the seeder is between 1.3-2 % of the total mass flow.

Due to high intensity scattering signal of spray ligaments and droplets during the operation of the atomizer, the selection of tracer particles with a high signal to noise ratio is of particular importance. Simultaneously a notch filter(Edmund notch filter) is used to seperate the emitted light of $BAM : Eu^{2+}$ tracers($\lambda = 450\,\mathrm{nm}$) and the scattered light of liquid phase($\lambda = 355\,\mathrm{nm}$).

A series of 200 instantaneous double frame images is recorded for each OP. The recordings are post processed using a commercial PIV algorithm (software: LaVision, DaVis 10.0) and averaged to display the mean velocity field near the

atomizer. An initial interrogation window of 128 × 128 pixels (1.07 × 1.07 mm) and a final size of 48 × 48 pixels (0.4 × 0.4 mm) is used with an overlap of 50 % and 75 %, respectively. A rectangular and a circular weighting function is applied for the initial and the final window size, respectively.

Shadow Imaging

Background Shadow Imaging is a background illumination technique often used for the visualization of liquid flows and for quantitative spray analysis. The same laser setup, camera and repetition rate (i.e. 10 Hz) is used for both, PIV and Shadow Imaging. For Shadow Imaging, the laser beams are expanded using a spherical lens and directed onto a fluorescent screen. The fluorescent screen emits a diffused red shifted light, which is used for the background illumination.

The camera is equipped with a Nikon macro lens with a focal length of 200 mm to obtain an overall view of the primary breakup mechanism. The resulting FOV is approximately of the size 27 mm × 18 mm and the pixel resolution is calculated with 8.3 µm per pixel. The optimum pulse separation is Δt = 10 µs.

Measurement Locations

The measurement locations are shown in Fig. 2 and 3. The origin of the coordinate system is defined at the atomizer orifice. The vertical axis of the flow channel is defined as the y-axis and the radial direction is defined as the x-axis. PIV and Shadow Imaging are performed in the FOV marked bluish in Fig. 2 and 3, yet with a slightly shifted overlap. For both measurements, the origin is used as the reference point for relative spatial translation through the flow channel. The measurements are conducted at five equidistant axial offsets (y_{1-5}) to one side of the spray cone, i.e. assuming axial symmetry. The exact measurement of positions of both procedures are listed in Tab. 2. For the Shadow Imaging the last axial measurement height is chosen due to the breakup length of the liquid sheet. Thus, y_5 is directly located at the edge of the primary breakup zone. For PIV measurements a wider range of equidistant positions is choosen to take the more downstream areas into account as well.

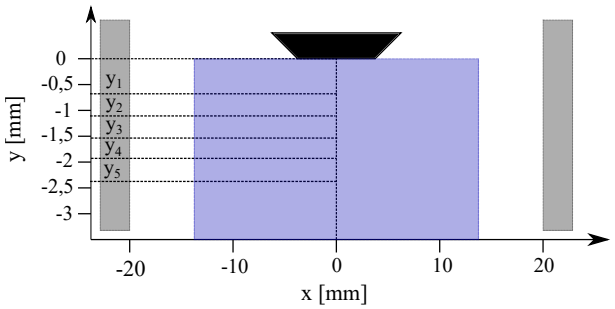

Figure 2: **Spatial measurement locations for Shadow Imaging; location of origin (x, y = 0) at the atomizer orifice**

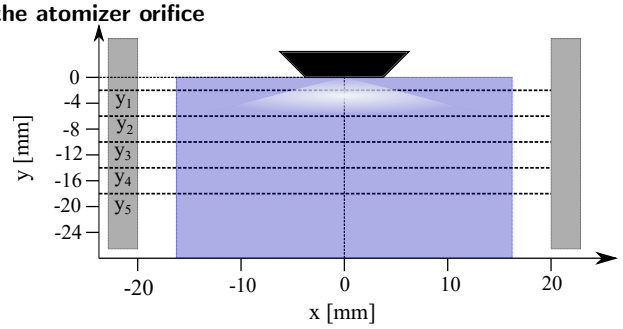

Figure 3: **Spatial measurement locations for PIV; location of origin (x, y = 0) at the atomizer orifice**

METHODOLOGY

Calculation of Breakup Length, Spray Angle and Statistical Growthrate

For the calculation of breakup length, spray angle and statistical growthrate, the raw instantaneous shadow images are post processed to gain statistical information from 500 single records. Figure 4 shows a raw instantaneous shadow image and the corresponding post processed data for breakup length and spray angle calculation. The normalized raw image is first binarized using a fixed threshold for all series. Schäfer et al. [**?**] shows in his investigations that a factor of 0.95 for binarization provides reliable results. The binarized pictures allows to describe the liquid contour with a fourth order polygon, which has a derivative of zero at maximum or minimum amplitude. Therefore a mean amplitude in each operating point can be determined. With repsect to the equidistant

	Shadow [mm]	PIV [mm]
y_1	0.72	2
y_2	1.13	6
y_3	1.53	10
y_4	1.94	14
y_5	2.34	18

Table 2: **Axial measurement locations for Shadow Imaging and PIV measurements**

positions in Fig. 2 a relativ amplitude in reference to the symmetric axis(x_0) and mean amplitude can be calculated. The breakup length is calculated as the distance between (x_1, y_1) or (x_2, y_2) and the origin (x_0, y_0) at the atomizer orifice. The spray angle is defined as the angle between the two resulting lines of the breakup length.

Calculation of Turbulent Kinetic Energy

For the calculation of turbulent kinetic energy the PIV pictures are post processed with LaVision 10.0. As likely above the origin is at the atomizers orifice (x_0, y_0). For each OP a series of 200 pictures is utilized, axial and radial velocity vectors are determined. In order to guarantee a statistical relaibility vectors with a lenght below 50 become neglected. In a next step the mean velocity components u' and v' are determined with the sum of the mean and fluctuation velocity normalized with maximum vector length. Therefore turbulent kinetic energy can be calculated by the two dimensional formular as

$$k = \frac{1}{2}\sqrt{2u'^2 + v'^2}.$$

In comparison to an injection in a quiescent and moving air the post processing has similar parameters for the adjustable filter width ($L = 51px$) in DaVis 10.

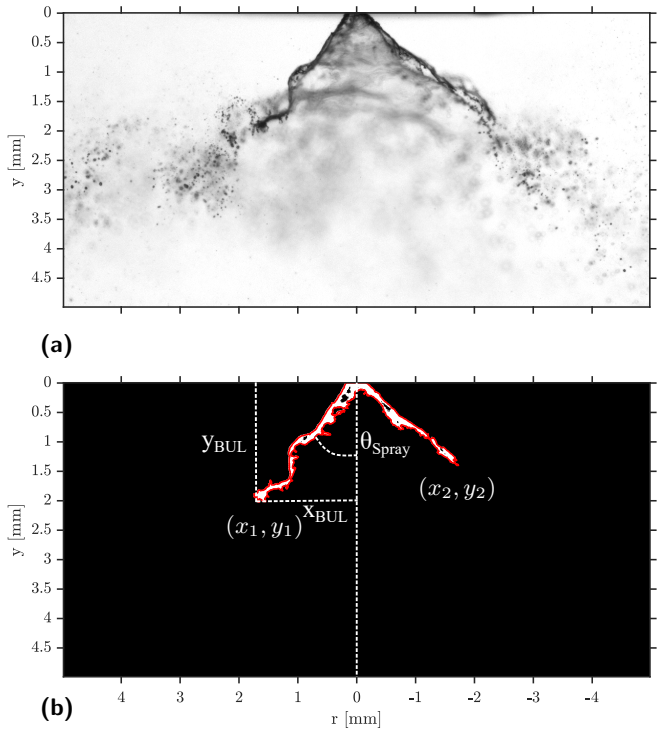

Figure 4: (a): Raw shadow image of primary breakup; (b): Processed shadow image for breakup length and spray angle calculation

RESULTS AND DISCUSSION

The average air flow fields for the cases with and without a spray are displayed in Fig. 6. Images in (a) show the case for low co-flow air of 20 m/s (OP20) without injection and (b) the case at 20 m/s (OP20) with a fully formed hollow conical spray. The cross section of the atomizer is indicated as a gray box at the top. The origin of coordinates is choosen for y = 0 mm at the nozzle orifce and the radial origin with r = 0 mm is in the symmetric axis of the injector in reference to Fig. 1. The air flow direction is from top down. The colored background indicates the velocity magnitude and the overlaid streamlines indicate the flow direction of the air.

It is evident that the primary break up process is strongly affected by the co-flowing air. In consideration of the distortions growth rate on the liquid surface

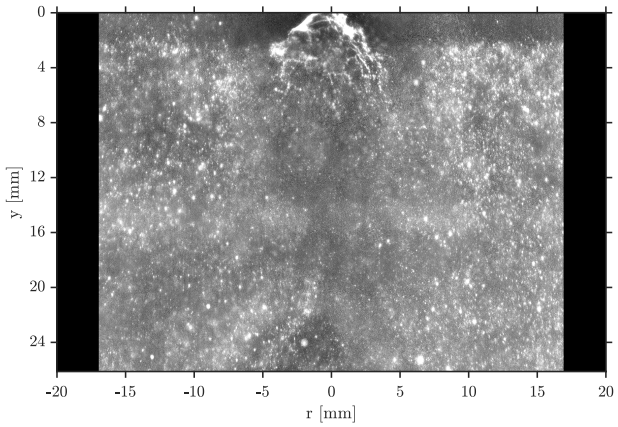

Figure 5: Raw PIV image at OP20 and $\dot{m}_{Spray} = 0,4\,g/s$ for Delavan injector

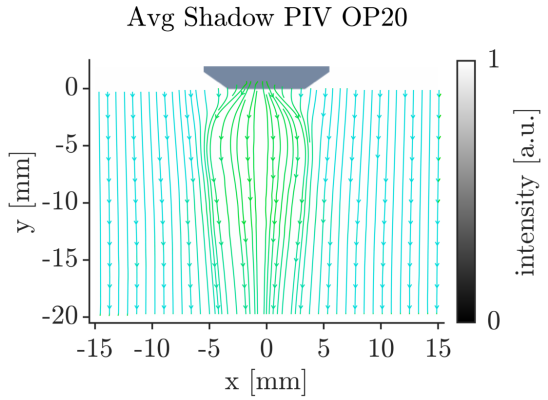

Figure 6: Averaged air flow field in OP20 with spray

and the break up length significant changes for higher momentum of coaxial airflow may be observed.

For all three cases, a two-sided interaction between the fluid and the coaxial airflow can be observed close to the atomizer orifice. The air vortex is located on the outer side of the gas-liquide interface (GLI) at approximately y = 2 mm, which results in a deflected streaming of air towards the wall of the test section. The momentum of the distraction vortex is dependent on the co-flow velocity and y-position. With increasing bulk velocity of the co-flow, the magnitude of turbulent kinematic energy in the area around the GLI (r = ±5 mm) increases

for OP20, 50, and 80, respectively. The deflected air-flow influecences additionaly the growth-rate of the Kelvin-Helmholtz instabilities. Therefore the break

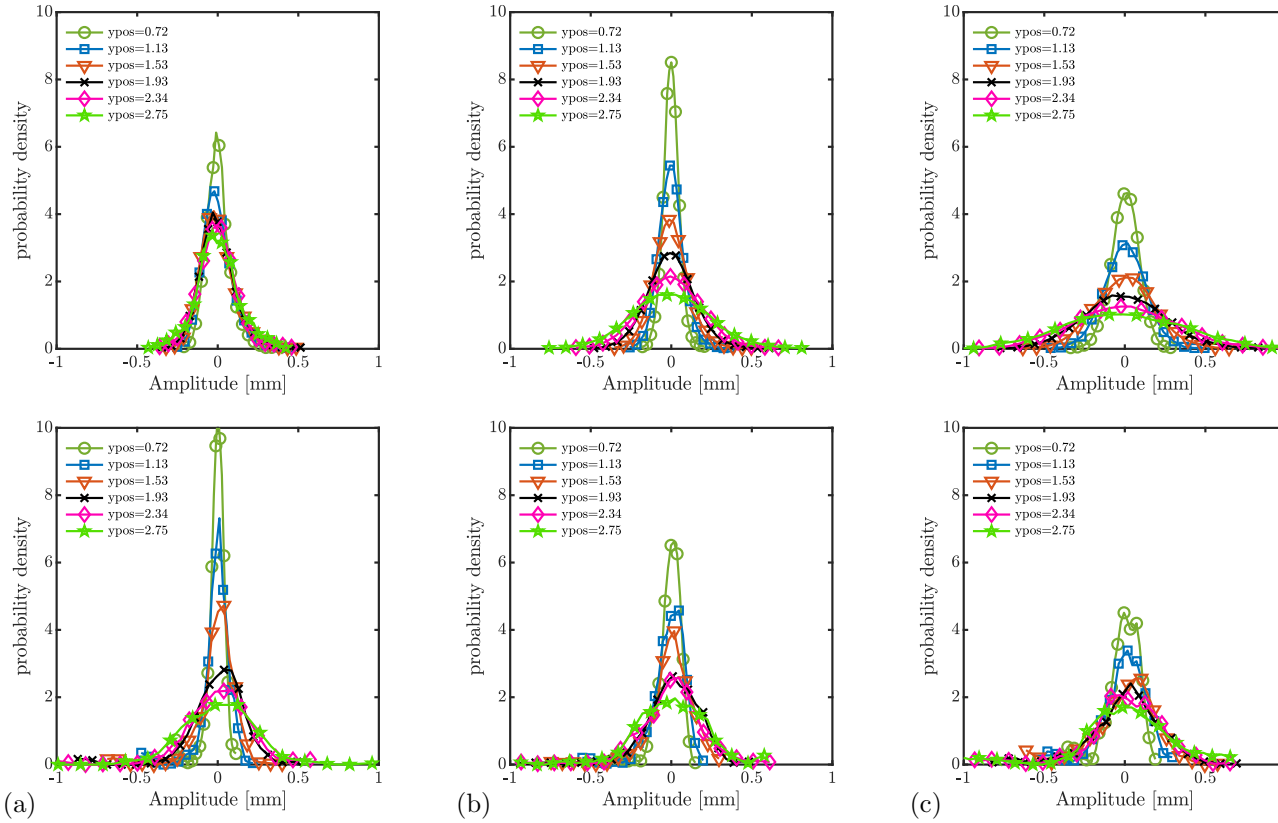

Figure 7: **Statistical distribution of distortion amplitude for Delavan (top) and Schlick (bottom) injector: (a) OP0; (b) OP5; (c) OP8**

At high air velocities the influence on the spray cone is intensified by an pressure drop at the nozzle exit due to a lower static pressure in the free stream, which leads to a broadening of the spray cone angle for increasing co-flow velocities[Quelle:Fu et al.]. Therefore the widend sheet surface sees more of the coaxial air stream and this mechanism is resulting in higher Weber numbers.

Influence on Primary Breakup

As discussed above, the high co-flow velocities are exciting distortions on the sheet surface which leads to higher amplitudes and therefore shortened liqiud sheets. For a quantitativ discussion we are considering the statistical distribution of amplitudes at the positions in Fig. 2. The Fig. 7 shows the statistical reltiv amplitude for both investigated injector types. Basically a significant behavior can be detected, the height of the relativ amplitude increases for further downstream positions. In comparison to higher co-flow rates like in OP20, 50 and 80 the function of the standard derivation gets widend, which confirmes the approach of excitation of distortions with a higher momentum airflow. Both injectors can be distinguished in their orifice geometry, for example the Delavan injector has a trompet outlet and the Schlick injector has not. In the next Fig. 8 the fluctuations of the radial component of breakup length are displayed. Its described as a cumulativ destribution function (CDF).The value on the vertical axis is defined as a statistical amount of detected sheets. A value of one shows that all sheets of the series (500 pictures) are detected. On the other hand side the value zero indicates no sheet is detected at this position. For every OP the distribution is plotted, a steep gradient represents a diluted fluctuation in the radial component of breakup length. For the Delevan injector the CDF shows an increase of the radial component of BUL in OP 20. The maximum slope gradient is about 0.00971/mm. In the higher OP's the BUL shortens, and the gradient gets steeper. For example in OP 80 the radial component of BUL is equal to OP 0 and exhibits a maximum gradient of 0.01031/mm. It may be concluded a damped fluctuation for upper OP's. In comparison to the Delavan, the Schlick injector shows basically a similiar behaviour. For increasing co-flow velocities the BUL decreases. A conspicuous feature is the difference in the development of maximum gradient for higher OP's. In OP 0 and 50 a nearly equal maximum gradient can be detected. For OP 0 the maximum gradient is about 0.0257/mm and for OP 50 0.0258/mm. In the upper OP, OP 80 the maximum gradient is around 0.0239/mm. In this case the fluctuation of the radial BUL component is increasing.

OP	stat. growthrate [-]	Breakuplength [mm]	half spray angle [◦]
20	0.01291	2.422	35.05
50	0.01523	2.214	37.36
80	0.02134	1.909	39.19

Table 3: **Shadowgraphy results for Schlick injector at T_∞= 298 K and $\Delta p = 11*10^5$ Pa.**

For a better conclusion of the discussed charactristca above, the results of the primary breakup shadowgraphy are displayed in Tab. 3 and Tab. 4. For the

OP	stat. growthrate [-]	Breakuplength [mm]	half spray angle [◦]
0	0.01329	2.199	48.62
20	0.005559	3.691	50.19
50	0.02096	3.219	53.62
80	0.05106	2.181	54.52

Table 4: **Shadowgraphy results for Delavan injector at T_∞= 298 K and $\Delta p = 2.6*10^5$ Pa.**

both investigated injectors a similiar trend is detected. With an increasing co-flow velocity the statistical growthrate of distortion grows, this underlines the hypothesis of excitation due to distracted airflow at the GLI. The half spray cone angle gets broaden for OP 20; OP 50 and OP 80 respectively. The numerically higher values for the Delavan injector in the spray cone angle is attributed to the trompet geometry of the orifice.

Gas-liquid interaction of a liquid spray in coaxial flow

For an enhanced comprehension of the bilateral influences between the fully formed liquid spray and coaxial flow, the flow field is investigated with a specific

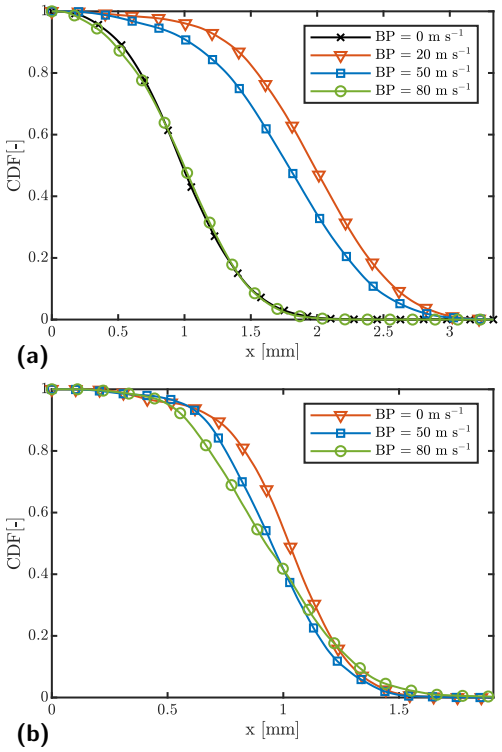

Figure 8: Cumulative distribution function of radial component of BUL for (a) Delavan and (b) Schlick injector in OP 0; OP 50 and OP 80

and modified PIV technique. In the case of a multiphase flow the conventional method of PIV does not provide satisfying results. Thereby a challenging issue, as discussed above in this Section, is the intensive mie scattered light of the liquid phase, which leads to an overexposed image without any evaluable information about the seeded airflow. As written in Section a few modification on the test section were made, and the selection on feasible tracer, like [abram] investigated already, is vittaly important. The initial hypothesis that the coaxial-flow is deflected by the conical liquid spray in the region around the GLI has to be proven. According to that the flow field is investigated at the positions in Table 3 and profiles of mean velocity fluctuation in radial and axial direction are plotted and interpreted. In addition the turbulent kinetic energy is considered at the positions respectively. In general the coflow velocity is varified as well

and especially the cases with spray and without are faced.

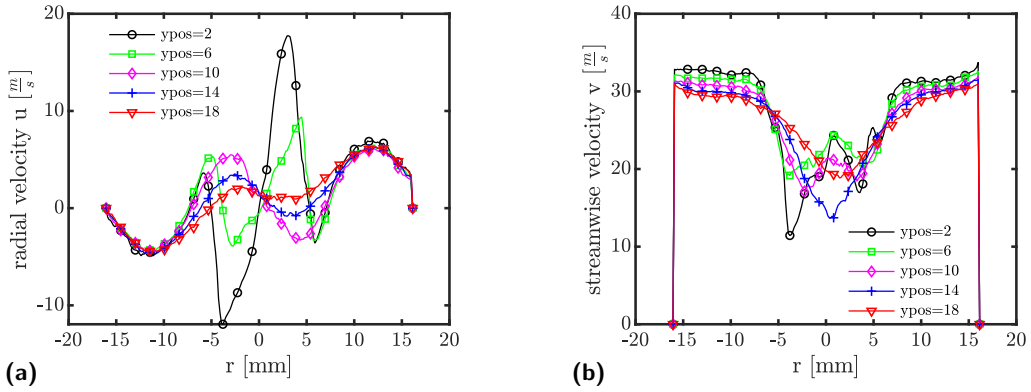

Figure 9: Velocity profiles at positions in Table 3 with spray for Schlick injector in OP 20 (a) radial and (b) axial velocity

In Fig 9 the normalized radial and axial velocity components are displayed for OP 20 with Schlick injector. By definition a change of sign defines a change in the direction of the radial component. For the dircetion towards the center line of the test section a positiv value is defined. Accordingly a negative value declares the oppsite direction. It is shown for the profiles close to the nozzle exit y = 2 mm, at the radial position of r = ± 5 mm the co-flow gets deflected by the liquid sheet. This effect can be detected as two symmetrical peaks in the profil at r = ± 5 mm. For the downstream position at y = 6 mm a similiar behaviour is shown. Only the numerical magnitude differs from the profil at y = 2 mm, it decreases. At the positions in the spray wake, the signficant peaks vanishes. A more flatten velocity profil is plotted. This may be seen as an indicator for breakup and therefore the two phases have mixed up. In Fig. 9 (b) the axial velocity profils is displayed. In consideration of the local gradient at the GLI (r = ± 5 mm, y = 2 mm) a steep gradient represents a high deceleration of the axial velocity component. In the wake of the spray a more flatten gradient

shows an aligned destribution of axial velocity to the co-flow. In addtion to Fig. 9 the radial and axial components for the Delavan are investigated. Especially, two cases with and without a spray in OP 20 are discussed. The correspondig profiles are plotted in Fig. 10 (a) without spray and (b) with spray. The difference in the charactersistical slope at position y = 2 mm for the two cases is faced definitely. The radial component with no spray, does not show a a double change in sign, only the wake of the injector contour is shown as a change in direction at r = ± 5 mm. In Fig. 10 (b) the radial componenten for the case with spray, owns the same slope curvature as the Schlick injector. Two symmetrical peaks can be detected at the same radial position. The outer diameter of the injector is $d_0 = 10$ mm as well. Also the decrease in magnitude for further downstream positions like y ≥ 10 mm is similiar. At this position the slope curvature does not differ from the slope without a spray. Therefore mixing of the liquid and gas phases is fully developed. At this point the comparision of the two cases for the axial component delivers same results as for the Schlick injector. A steep gradient in the area of the GLI is represented, for the case with a spray. In reference to this, the interface position and the influences on the co-flow can be estimated. Also the decrease in the magnitude is significant for the case with a spray.

The comparison of the turbulent kinetic energy for both injectors is constituted in Fig. 11 and Fig. 12. As it is displayed in both Figures the symmetrical peaks for OP 20 at r = ±5 mm can be detected. Apparently in this area of the GLI the air stream gets deflected and a turbulent air stream results. It is also shown, that the numerical magnitude of the turbulent kinetic energy, $k = 6\,m^2/s^2$ for both injector types is almost equal in OP20. In addition, for further downstream positions y ≥ 10 mm the peaks at r = ± 5 mm vanishes and a single symmetrical expanded peak appears. For example, the energy for the Schlick injector at y = 14 mm is about $k = 4\,m^2/s^2$ and decreases if y increases. Apparently the breakup takes place at y ≥ 10 mm and a fully turbulent wake is formed. For the Delavan injector a similiar characteristica is investigated. In general the spraycone angle of this injector is broader spread, this is shown in

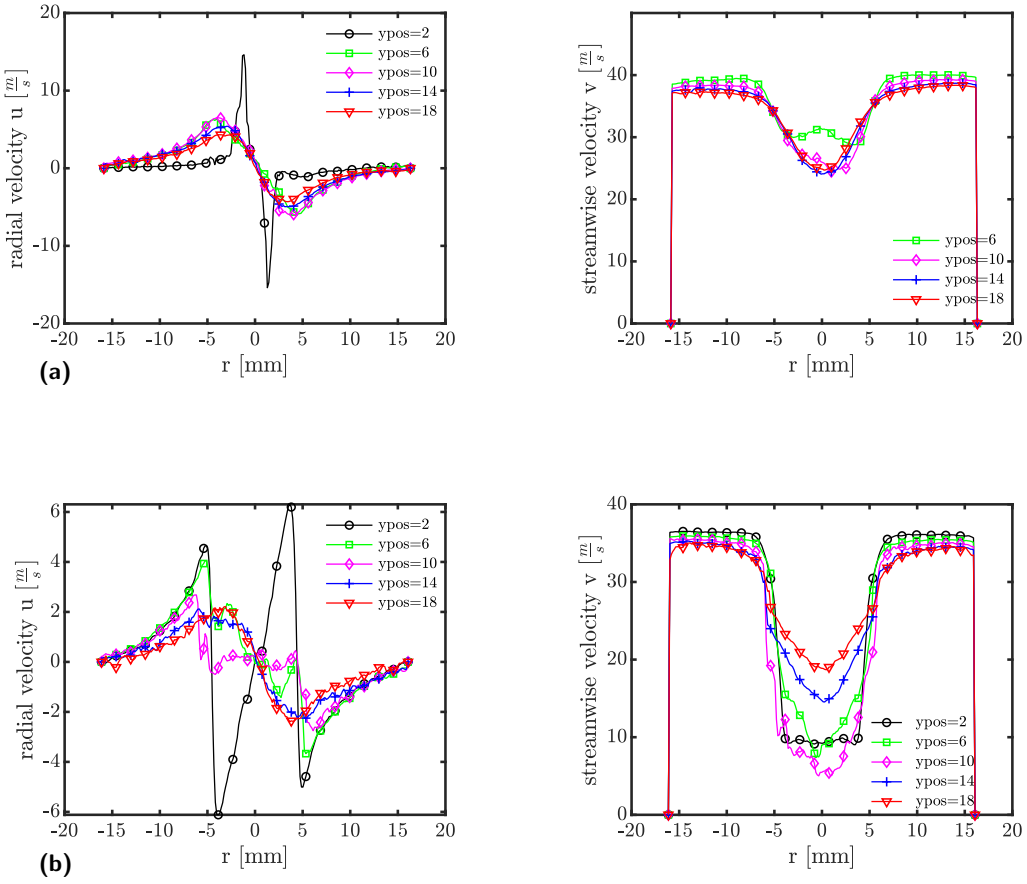

Figure 10: Axial and radial velocity profiles at positions in Table 3 with and without spray for Delavan injector in OP 20 (a) without spray (b) with spray

Table 4 for example. In comparison of the peak positions in OP20, it can be retained that for the position y = 2 mm the peak is at r = ±5 mm and for y = 10 mm the peaks are shifted to r = ±6 mm symmetrically. This is consistent with the a larger BUL for the Delavan injector. For downstream positions y ≥ 10 mm no peaks are shown, thus it is evident that break up takes place around y = 10 mm in OP20. In Fig. 12 (b) the turbulent kinetic energy in OP 20 for the Delavan injector without a spray is presented.

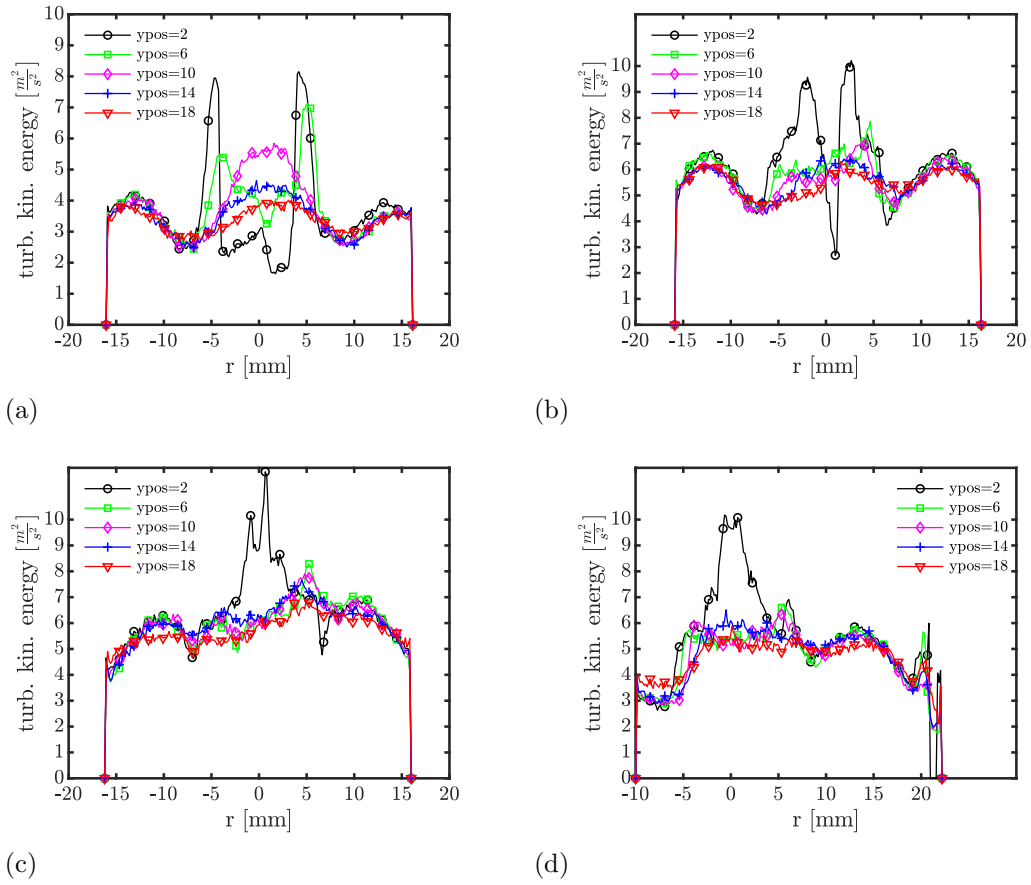

Figure 11: **Turbulent kinetic energy for Schlick injector (a) OP20; (b) OP50; (c) OP80 and (d) OP80 at wall**

The plots for several downstream positions are not showing the character-

istical symmetric peaks at the area of the outer injector diameter r = ±5 mm. There is a single peak in magnitude, which represents the injector wake. For example at y = 2 mm the turbulent kinetic energy is k = 6.5 m^2/s^2. For further downstream positions y ≥ 2 mm the numerical magnitude decreases and the width of the peak as well. Therefore the origin of this peaks is an unambiguous evidence for a defelection of the co-flow by liquid spray. In higher OPs the significant peaks are not clearly shown. For OP 50 at y = 2 mm the symmetrical peaks at r = ±5 mm can be identified but for further downstream positions the wake is already fully developed. Due to the shorten BUL the bilateral interaction of co-flow and liquid spray takes place earlier in more upstream positions, which can be not visualized in the investigated FOV. As it is shown in Fig. 12 (e) no peaks are visible, due to the early upstream breakup. In general the magnitudes of turbulent kinetic energy are round about k = 5.5 m^2/s^2 for the spray wake at positons for y ≥ 10 mm and the wake caused by the injector geometry. These values are numerical steady for each OP. Especially for OP 20 the significant behaviour which was assumed, can be proven for both injector types. The quality of subsequent behaviour for the tracer particles can be estimated with the Stokes number. For the used $BAM : Eu^{2+}$ tracers with an mean diameter of d_p = 2-3 μm [**?**] a Stokes number of $St_{OP20} = 0.075$ for OP 20 and $St_{OP80} = 0.3$ for OP 80 results. A Stoke number of St≪1 represents a reliable subsequent behaviour[].

References

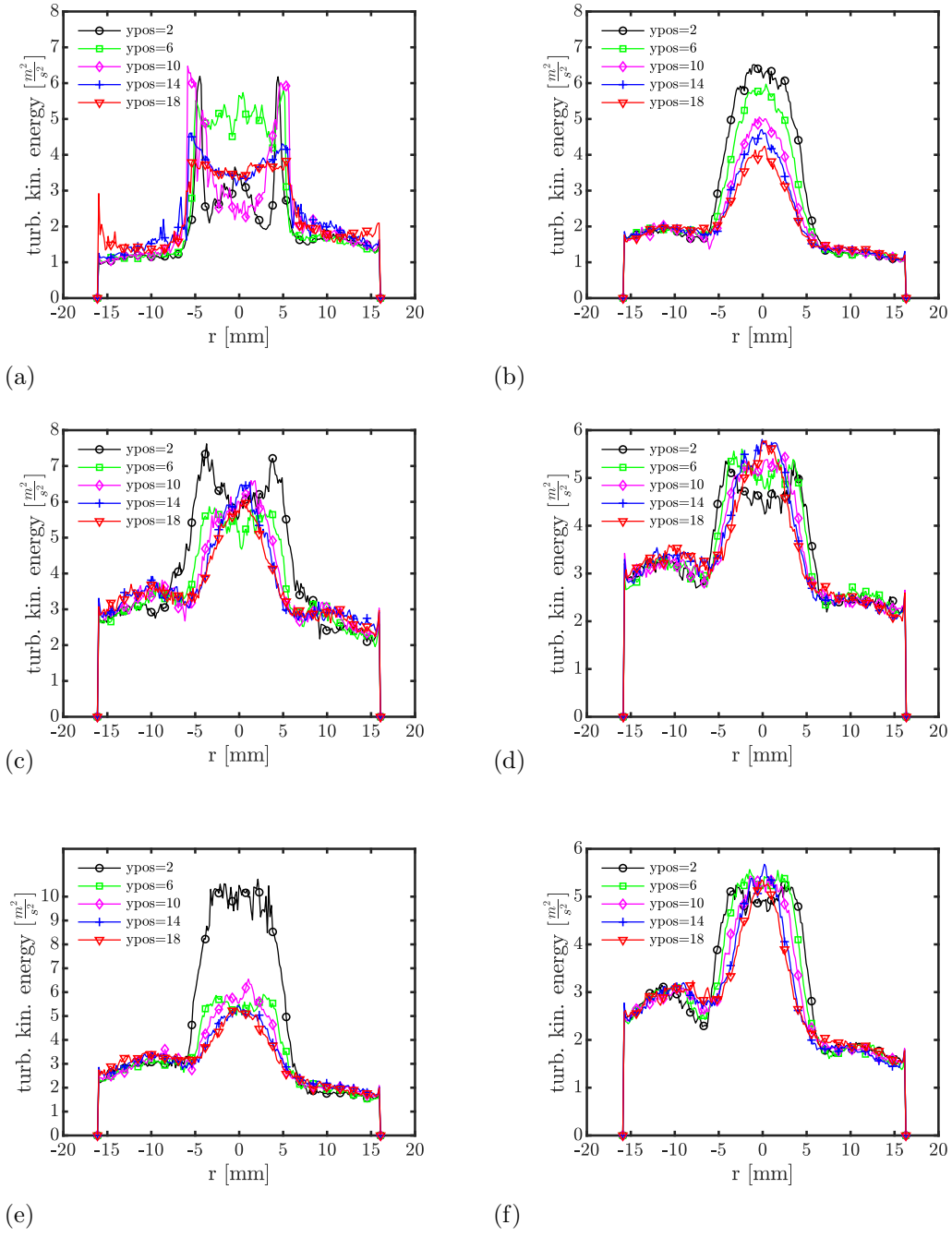

Figure 12: **Turbulent kinetic energy for Delevan injector (a) OP20; (c) OP50; (e) OP80 with spray and (b) OP20; (d) OP50; (f) OP80 without spray**